International Journal of Mechanical Engineering and Applications
2025, Vol. 13, No. 3, pp. 86-97
https://doi.org/10.11648/j.ijmea.20251303.11

Research Article

Integrated Free-bulge Forming Method for Thin-walled Metallic Spherical Cap Structures

Junfu Hou[1], Lingzhe Meng[1], Chenghai Kong[2], Jingchao Guan[3], Wei Zhao[4, *], Xilu Zhao[1]

[1]Department of Mechanical Engineering, Graduate School, Saitama Institute of Technology, Saitama, Japan

[2]Topy Industries Co., Ltd., Aichi, Japan

[3]International Operations Division NAVIC Co., Ltd. Aichi, Japan

[4]Department of Mechanical Engineering, National Institute of Technology Toyama College, Toyama, Japan

Abstract

The end surfaces of large storage tanks used in various industries are often composed of thin-walled metallic spherical cap structures. The ability to process these components at a low cost and with high manufacturing precision is an important research challenge. In this study, a new integrated free-bulge forming method is proposed to fabricate thin-walled metallic spherical cap structures. This method involves fixing the perimeter of a circular forming sheet, applying internal water pressure, and uniformly bulging the central portion of the sheet to achieve a spherical cap structure. To analyze the forming performance of the proposed method, formulas for calculating the plastic strain and average thickness during the process of forming the spherical cap from the circular sheet are derived, enabling a clear understanding of the workable range of the free-bulge forming method. Additionally, by deriving a prediction formula for the internal water pressure required for the free-bulge of the spherical cap structure, the key process design factors are identified. For verification, a free-bulge forming device is developed, and thin-walled metallic spherical cap structures are processed. The results confirm that the spherical cap shape is sufficiently precise and can be stably produced using the free-bulge forming method. Furthermore, a specialized device for measuring the shape accuracy of the spherical cap formed using the proposed free-bulge method is developed, and the surface shape of the spherical cap structure is measured. The results show that the formed spherical cap shape has a maximum deviation of 2.3% from the theoretical shape, demonstrating adequate precision for practical applications. To further verify the processing performance of the free-bulge forming method, the thickness distribution of the processed thin-walled metallic spherical cap is measured along its diameter. The results show that, compared to the original thickness of 1.0 mm, the minimum thickness of 0.858 mm occurs at the center of the spherical cap, representing a thickness reduction rate of -13.2%. It is confirmed that the free-bulge method can be stably applied to typical thin-walled press materials.

Keywords

Spherical Cap Structure, Free-bulge Forming Method, Storage Tank, Spherical Shell, Metal Forming Sheet, Plastic Formability

*Corresponding author: zhaowei@nc-toyama.ac.jp (Wei Zhao)

Received: 3 April 2025; **Accepted:** 15 April 2025; **Published:** 14 May 2025

1. Introduction

Large storage tanks are commonly used for natural gas, oil, and other substances. Due to the flammability of their contents, particularly when placed in complex natural environments, the design, manufacturing, and safety issues of storage tanks have received significant attention [1-5]. There are many different types of storage tanks, which vary depending on their intended use [6-8]. Considering factors such as earthquake resistance, safety in response to natural disasters, and daily operational management, numerous studies have been conducted on the design and development of storage tanks [9-13]. To better understand stress distribution and other mechanical properties of storage tanks, finite element method (FEM) simulations have been performed [14-16]. These research results provide a valuable foundation for the design and development of storage tanks.

However, from the perspective of manufacturing industrial storage tanks or daily operational management, head components composed of curved parts are attached to the end faces of large storage tanks. Furthermore, from the viewpoint of material utilization and the mechanical properties of the storage tank, it is most common to use a hemispherical shape as the head component.

A spherical cap is the smaller part of a spherical shell created by cutting a sphere into two parts with a plane. When the plane passes through the center of the sphere and the height of the spherical cap is equal to the radius of the sphere, it forms a hemisphere.

The processing of thin-walled metallic spherical cap structures is an important research topic, similar to the processing challenges associated with storage tanks [17-19]. Sequentially welding pre-formed curved parts is the most common method of producing thin-walled metallic spherical structures. Consequently, issues related to crack formation in welded thin-walled metal storage tanks have been addressed [20-23]. Additionally, the residual stress generated during welding significantly affects the fatigue strength of storage tanks; thus, research on the distribution of residual stresses in welded structures has been investigated [24-26].

Furthermore, methods utilizing the hydraulic plastic deformation of thin-walled metallic materials have been proposed and developed to reduce the manufacturing costs and improve the quality of storage tanks [27-29]. Most research on hydraulic forming has focused on processes that involve integrated bulge forming for spherical tanks [30-32]. However, the manufacturing of components such as spherical cap structures for storage tanks has received limited research attention.

In this study, a novel free-bulge forming method that can be easily implemented is proposed for the processing of thin-walled metallic spherical cap structures used on the end faces of spherical or cylindrical storage tanks. To put the proposed free-bulge forming method to practical use, both geometric and mechanical theoretical factors are considered. A free-bulge forming experimental device for thin steel plates is developed, and actual processing experiments for spherical cap structures are conducted. Detailed studies are conducted on the specific processing conditions, shape accuracy of the processed products, and their mechanical properties.

2. Materials and Methods

2.1. Spherical Cap Structures and the Free-bulge Forming Method

Spherical and cylindrical storage tanks, as shown in Figure 1, are widely used in various industries. For manufacturing or cleaning purposes, a thin-walled metallic spherical cap is required, as indicated by the shaded area in Figure 1.

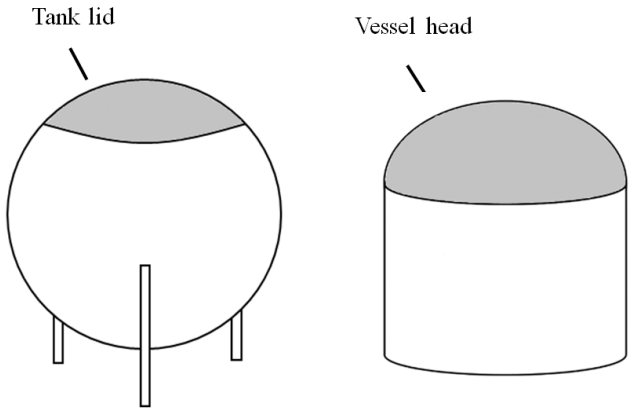

Figure 1. *Spherical and cylindrical industrial storage tanks.*

The conventional processing method shown in Figure 2 is typically used to process the thin-walled metallic spherical cap structures shown in Figure 1.

Figure 2 (a) illustrates a spinning process, where the central part of the circular workpiece is pressed and fixed onto the center of the molding die. While rotating both the molding die and workpiece, a forming roll is then pressed against the workpiece to continue local plastic forming in the circumferential direction, gradually shaping the spherical cap structure. The limitations of this processing method are that it requires specialized equipment and forming jigs, and the maximum diameter of the processed spherical cap structure is limited, making it difficult to process large spherical cap structures.

Figure 2 (b) illustrates the partial part welding method. First, the partial parts are pressed and processed into curved surface parts. Using a circular positioning jig, the curved surface parts are individually welded to form the entire

spherical cap structure. The limitation of this processing method is that a press machine and forming die are required to process curved surface parts. Additionally, a positioning jig is required during the welding assembly process, and it is difficult to ensure the shape accuracy of the resulting spherical cap structure.

To address these limitations and process spherical cap structures with a simplified processing flow and relatively low processing costs, this study proposes an integrated hydroforming method, as shown in Figure 3. First, the boundary of the circular thin plate is fixed before hydraulic pressure is applied to the center of the circular thin plate, causing the center to bulge and form a spherical cap structure.

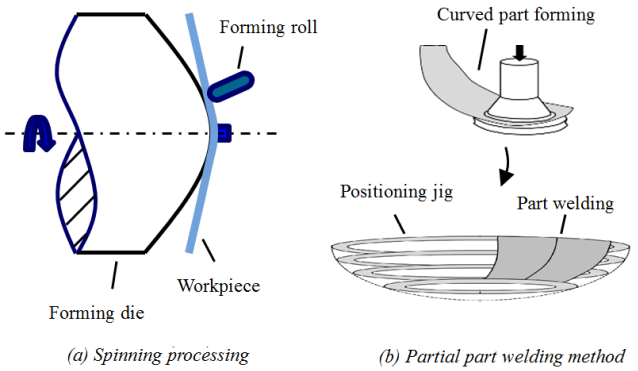

Figure 2. *Conventional processing method for thin-walled spherical cap structures.*

In the integrated processing method shown in Figure 3, the use of a completely uniform internal pressure for free-bulge forming contributes to the high shape accuracy of the spherical cap structures.

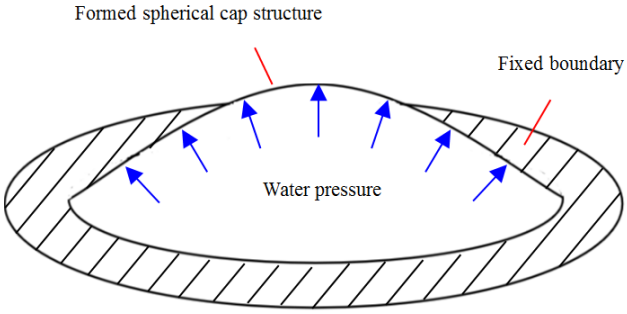

Figure 3. *Integrated free-bulge forming method for spherical cap structures.*

To implement the integrated processing method, a processing device was designed, as shown in Figure 4. The processing device consisted of three parts: an assembled molding set, a support frame, and a manual hydraulic pump. First, the ring-shaped jig, circular forming plate, and fixed base were securely connected using bolts and nuts. Next, the water inlet hole at the center of the fixed base was connected to a manual hydraulic pump via a hydraulic hose. Finally, using a manual hydraulic pump, water pressure was applied through the hydraulic hose to the assembled molding set, uniformly inflating the circular forming plate, thereby processing the spherical cap structure.

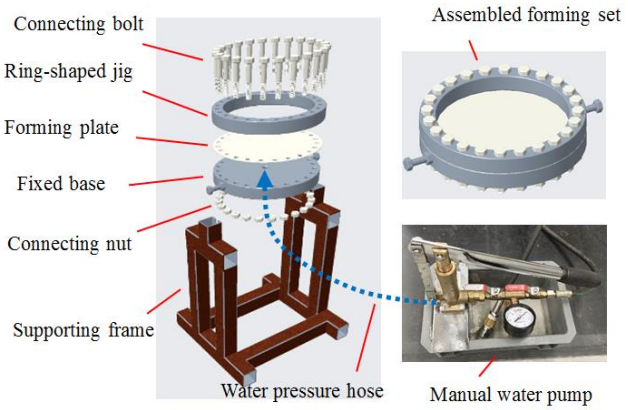

Figure 4. *Schematic of the integrated free-bulge forming equipment for spherical cap structures.*

Figure 5 shows a photograph of the integrated free-bulge forming device used to manufacture the spherical cap structure. As shown in Figure 5, a caliper was mounted on the door-shaped frame above the assembled molding set. The height of free-bulge forming was read in real-time from the liquid crystal screen of the caliper.

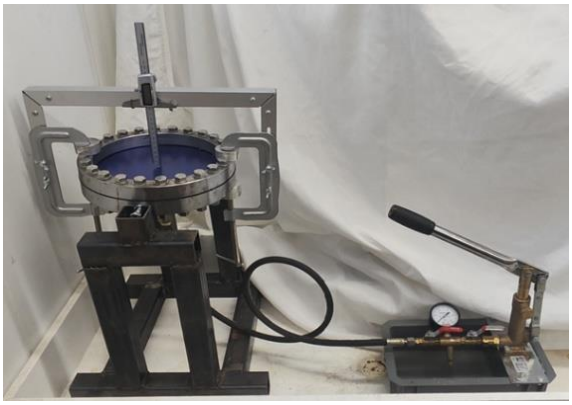

Figure 5. *Photograph of the integrated free-bulge forming equipment for spherical cap structures.*

As shown in Figure 6, the circular forming plate used in the prototype experiments in this study was made of Steel Plate Cold Commercial (SPCC). The diameter of the circular molding plate before forming was 300 mm, and the plate thickness was 1 mm. The diameter of the opening of the spherical cap structure after free-bulge forming was 250 mm,

and the forming depth was 45 mm.

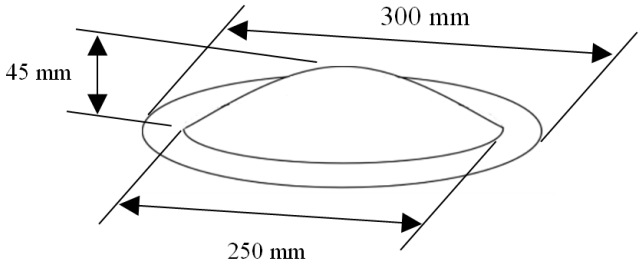

Figure 6. *Dimensions of the spherical cap structure produced by the integrated free-bulge forming method.*

2.2. Free-bulge Forming Analysis of the Spherical Cap Structure Equations

When processing a spherical cap structure with the shape shown in Figure 6 using a circular forming plate, the changes in the cross-sectional shape are shown in Figure 7. In Figure 7, the diameter of the circular molding plate before free-bulge forming was d = 250 mm and the free-bulge forming height was h = 45 mm. For the spherical cap structure: r is the radius, is the unfolding angle, and R is the chord length.

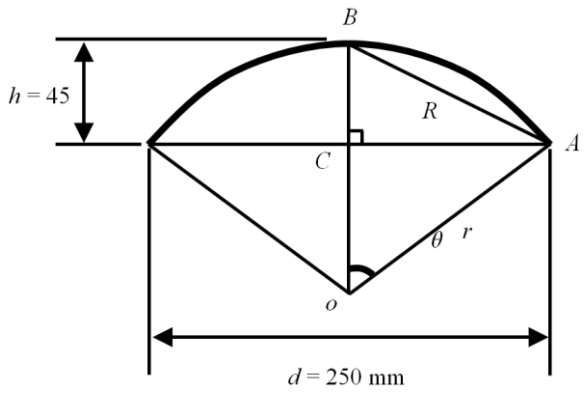

Figure 7. *Cross-sectional shape of the processed spherical cap structure.*

Based on the relationship between the isosceles triangle oAB, the formula for calculating the unfolding angle of the spherical cap structure is as follows:

$$\theta = 180° - 2\tan^{-1}\left(\frac{d}{2h}\right) = 180° - 2\tan^{-1}\left(\frac{250}{2\times 45}\right) = 39.6° \quad (1)$$

Based on the relationship of the right-angled triangle oAC, the radius of the spherical cap structure is expressed as follows:

$$r = \frac{d}{2\sin\theta} = \frac{250}{2\times\sin 39.6°} = 196.1\,mm \quad (2)$$

Based on the relationship of the right-angled triangle ABC, the chord length of the spherical cap structure can be expressed as follows:

$$R = \sqrt{h^2 + \left(\frac{d}{2}\right)^2} = \sqrt{45^2 + \left(\frac{250}{2}\right)^2} = 132.85\,mm \quad (3)$$

The area of the circular forming plate before free-bulge forming is expressed formulas follows:

$$S_0 = \frac{\pi d^2}{4} = \frac{3.14\times 250^2}{4} = 49087.38\,mm \quad (4)$$

The surface area of the spherical cap structure after free-bulge forming is expressed as follows [33]:

$$S = \pi R^2 \quad (5)$$

By substituting Equation (3) into Equation (5), the surface area of the spherical cap structure can be calculated as follows:

$$S = \pi\left[h^2 + \left(\frac{d}{2}\right)^2\right] = 3.14\times\left[45^2 + \left(\frac{250}{2}\right)^2\right] = 55449.11\,mm \quad (6)$$

Assuming that the material volume before and after free-bulge forming remains constant, and denoting the thicknesses before and after free-bulge forming as t and t_0 = 1.0 mm, respectively, the average plate thicknesses before and after free-bulge forming of the spherical cap structure can be calculated formulas follows:

$$t = \frac{S_0}{S}t_0 = \frac{49087.38}{55449.11}\times 1.0 = 0.89\,mm \quad (7)$$

The average rate of change in the plate thickness before and after free-bulge forming can be calculated formulas follows:

$$\frac{t - t_0}{t_0}\times 100\% = \frac{0.89 - 1.0}{1.0}\times 100\% = -11.0\% \quad (8)$$

When analyzing the shape changes before and after free-bulge forming of the spherical cap structure shown in Figure 7, it is assumed that the circumferential boundary of the circular forming plate is completely fixed. However, in practice, when performing free-bulge forming of a spherical cap structure, the material may flow slightly inward from the circumferential boundary of the circular forming plate. Therefore, the predicted values of the average plate thickness after free-bulge forming from Equations (7) and (8) are expected to be smaller than the actual average plate thickness

after free-bulge forming.

2.3. Prediction of the Internal Water Pressure for Free-bulge Forming

As shown in Figure 5, to perform free-bulge forming from the circular molding plate to the spherical cap structure, it is necessary to apply an internal hydraulic pressure using a manual hydraulic pump. To design the free-bulge forming process, it was essential to predict the required internal hydraulic pressure in advance.

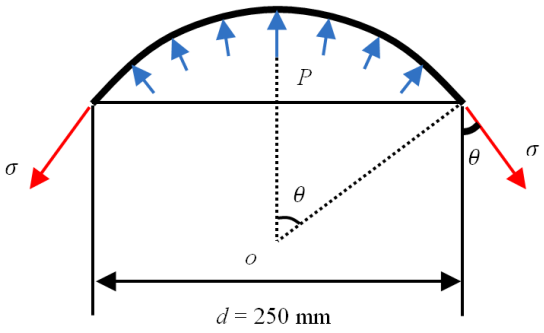

Figure 8. *Internal water pressure and stress distributions occurring during free-bulge forming.*

Figure 8 shows the distribution of the internal hydraulic pressure and stress that occur when free-bulge forming of the spherical cap structure is performed. From the equilibrium conditions along the symmetry axis direction in Figure 8, the following equation can be obtained:

$$P\frac{\pi d^2}{4} = \sigma \pi d t \cos\theta \tag{9}$$

Equation (9) can be rearranged as follows:

$$\sigma = \frac{Pd}{4t\cos\theta} \tag{10}$$

During free-bulge forming of the spherical cap structure, as the internal hydraulic pressure applied by the manual hydraulic pump gradually increases, the stress values also gradually increase. Plastic deformation begins when stress reaches the yield stress σ_y of the material. The internal hydraulic pressure at this point can be calculated as follows:

$$P = \frac{4\sigma_y t\cos\theta}{d} \tag{11}$$

In actual free-bulge forming, considering the effects of strain hardening in metallic materials, the internal hydraulic pressure applied from the manual hydraulic pump should be set approximately 20% higher than the predicted value calculated using Equation (11).

In the prototype experiments of this study, assuming a yield stress of 200 MPa for the SPCC, it was found that by setting the internal hydraulic pressure 20% higher than the predicted value from equation (11) at the point where plastic deformation occurred, the required internal hydraulic pressure for free-bulge forming was approximately 3.77 MPa.

2.4. Confirmation of Free-bulge Forming Quality Using FEM Analysis

To investigate the processing performance and practical feasibility in advance, FEM analysis was used to simulate the free-bulge forming process of the spherical cap structure, as shown in Figure 5.

Figure 9 shows the FEM analysis model of the circular forming plate. The circular forming plate was modeled using quadrilateral elements, with an average edge length of 2 mm for the quadrilateral elements, and the total number of elements was 14,193. The thickness of the circular forming plate was 1 mm. The material of the forming plate was SPCC, and the stress–strain curve of the material is shown in Figure 10.

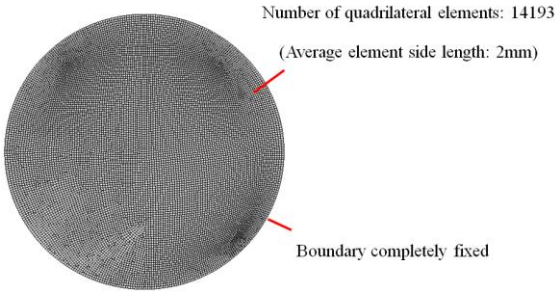

Figure 9. *Free bulge forming analysis model using FEM.*

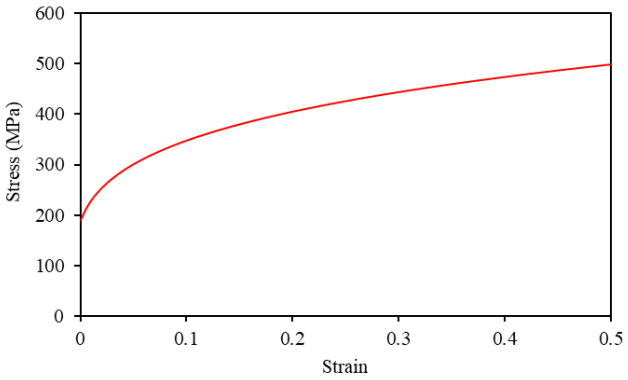

Figure 10. *Stress-strain curves of the free-bulge forming plate material.*

The results of the von Mises stress and plate thickness distribution at the completion of free-bulge forming obtained

from the analysis are shown in Figures 11 and 12, respectively. It was confirmed that because the internal hydraulic pressure was completely axisymmetric, free-bulge forming unfolded uniformly, resulting in the formation of a smooth spherical cap structure.

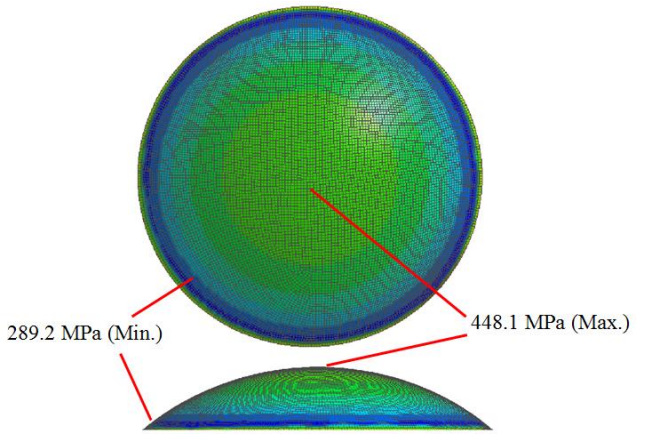

Figure 11. *Stress distribution in the free-bulge forming of the spherical cap structure.*

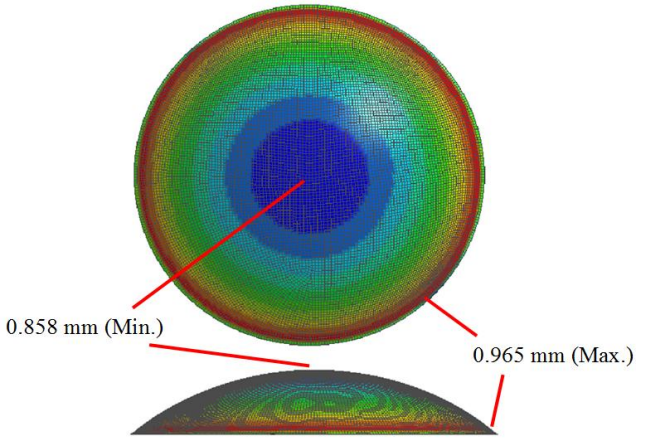

Figure 12. *Thickness distribution in the free-bulge forming of the spherical cap structure.*

According to the stress distribution results shown in Figure 11, the stress was axisymmetric along the vertical direction and centered around the symmetry axis. The maximum stress occurred at the center of the spherical cap shape, with a maximum von Mises stress value of 448.1 MPa. The minimum stress occurred near the surrounding fixed boundary with a minimum von Mises stress value of 289.2 MPa. Throughout the spherical cap shape, the von Mises stress exceeded the yield stress of the SPCC material, indicating that plastic deformation occurred.

According to the thickness distribution results in Figure 12, there was a slight tendency for the thickness to decrease uniformly across the entire surface compared with the pre-forming thickness of 1 mm. The thickness followed an axisymmetric distribution along the direction of the symmetry axis. The central part of the spherical cap shape was the thinnest, with a thickness of 0.858 mm and a thickness reduction rate of 14.2%. Near the surrounding fixed boundary, the thickness reduction was the smallest, with a thickness of 0.965 mm and a thickness reduction rate of 3.5%.

The maximum thickness reduction rate after the free-bulge forming of the spherical cap structure was approximately 14.2%, which was well within the plastic deformation limit of the thin steel plate. Therefore, it was confirmed through the simulation that when processing spherical cap structures made of SPCC material using this method, cracks did not occur and the forming process proceeded normally.

3. Results and Discussion

3.1. Free-bulge Forming Processing Experiment

To verify the free-bulge forming method of the spherical cap structure shown in Figure 5, parts of the actual processing experimental device and processing steps are shown in Figures 13 and 14, respectively.

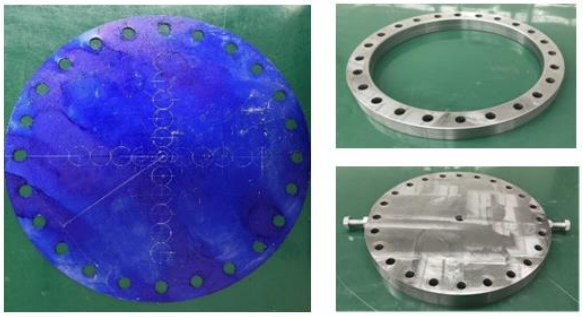

(a) Free-bulge forming set parts before assembly.

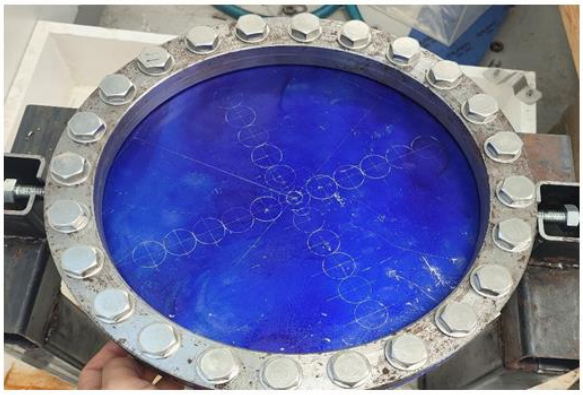

(b) Free-bulge forming set after assembly.

Figure 13. *Free-bulge forming set for the spherical cap structure.*

(a) Disassembly of the free-bulge forming set.

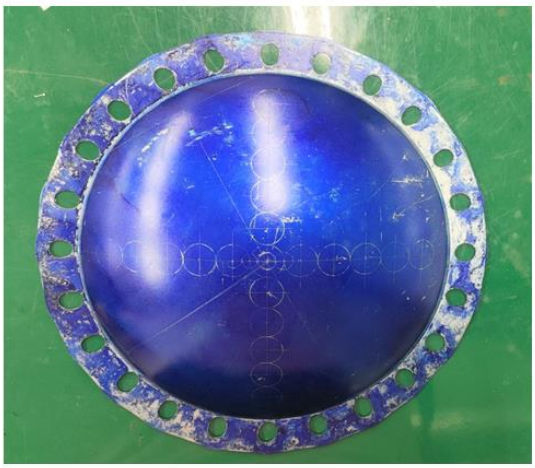

(b) Spherical cap structure obtained by free-bulge forming.

Figure 14. *Disassembly of the free-bulge forming set and the resulting spherical cap structure.*

Figure 13 (a) shows the circular forming plate, the ring-shaped jig, and the fixed base. 24 evenly distributed connecting bolt holes were drilled along the circular boundary.

To measure the plastic strain during the subsequent free-bulge forming process, the surface of the circular forming plate was sprayed with blue varnish and circular marks were drawn using a scribing tool. Figure 13 (b) shows the assembled molding set.

Figure 14 (a) shows the process of applying internal hydraulic pressure using a manual hydraulic pump and then disassembling the forming set with a wrench after plastic deformation due to free-bulge forming was completed. The actual internal hydraulic pressure required for the free-bulge forming was read from the meter of the manual hydraulic pump, and the maximum recorded pressure value was 3.65 MPa. This hydraulic pressure matched the predicted value calculated using Equation (11), confirming the consistency.

Figure 14 (b) shows the spherical cap structure obtained via the free-bulge forming. Figure 14 shows that, owing to the axisymmetric internal hydraulic pressure, the surface of the spherical cap structure formed by free-bulge forming became a smooth spherical cap structure.

Additionally, as shown in Figure 14 (b), the round bolt holes near the peripheral boundary of the circular forming plate before forming became elliptical holes after forming, and some of the metal in the flange area flowed inward. This phenomenon is advantageous as it helps to prevent the occurrence of cracks during free-bulge forming.

3.2. Plastic Strain in the Formed Spherical Cap Structure

To examine the quality of the spherical cap structure obtained through free-bulge forming, it was measured as shown in Figure 15.

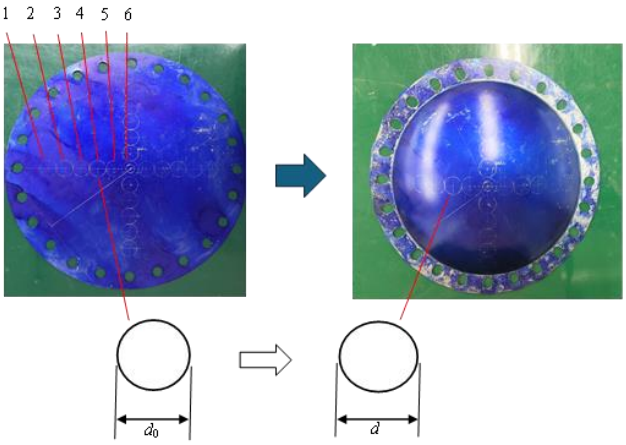

Figure 15. *Measuring the plastic strain of the spherical cap structure obtained by free-bulge forming.*

Before the bulge formation, as shown in the left diagram of Figure 15, circles were drawn on the surface of the circular-forming plate. After free-bulge forming, as shown in the right diagram of Figure 15, the circles from before free-bulge forming became ellipses, and the major axis d of the ellipse aligned with the diameter direction of the spherical cap structure. Additionally, as shown in the lower diagram of Figure 15, after measuring the diameter d_0 of the circle before free-bulge forming and the major axis d of the ellipse after free-bulge forming, the plastic strain at the central point of the circle can be calculated as follows:

$$\varepsilon = \ln \frac{d}{d_0} \tag{12}$$

However, to numerically estimate the plastic strain due to free-bulge forming, the cross-sections of the spherical cap structure before and after forming are shown in Figure 16. In Figure 16, the straight dashed line represents the diameter of the circular forming plate before forming, whereas the curved solid line represents the cross-sectional contour of the spherical cap structure after forming.

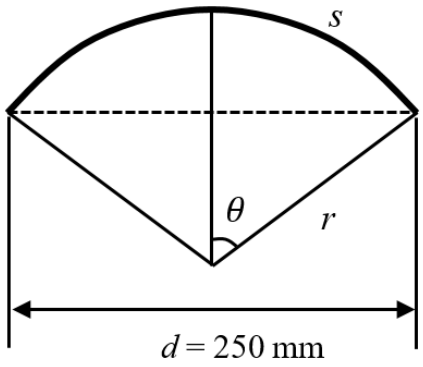

Figure 16. *Estimation of the plastic strain in the spherical cap structure.*

Using the equations for the expansion angle (Equation (1)) and radius (Equation (2)) of the spherical ca[structure, the length *s* of its cross-sectional contour line can be calculated as follows:

$$s = \frac{2\pi\theta r}{180} = \frac{2\times 3.14\times 39.6\times 196.1}{180} = 270.9\,mm \qquad (13)$$

Furthermore, using Equation (13), the plastic strain of the spherical cap structure after free-bulge forming can be approximately calculated as follows:

$$\varepsilon_a = \ln\frac{s}{d} = \ln\frac{270.9}{250} = 0.077 \qquad (14)$$

As shown in Figure 15, measurement points 1–6 were placed along the diameter of the spherical cap shape. The radii and major axes of the ellipses before and after free-bulge forming were measured at each point, and the plastic strain was calculated using Equation (12). To account for the repeatability and measurement accuracy, the radii and major axes before and after free-bulge forming were measured along four radii, as shown in Figure 15, and the average values of these measurements were used to calculate the plastic strain.

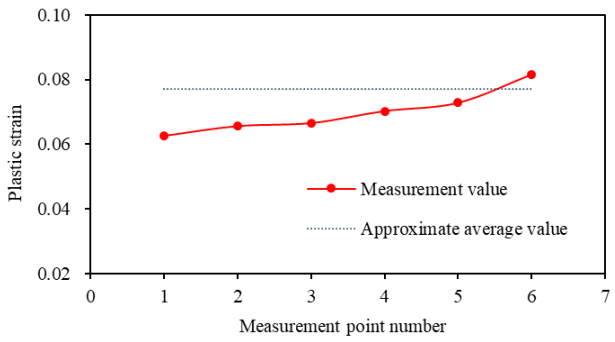

Figure 17. *Plastic strain distribution in the spherical cap structure obtained from free-bulge forming.*

For comparison, the measured plastic strain values of the spherical cap structure obtained from free-bulge forming and the average plastic strain values calculated using Equation (14) are summarized in Figure 17. In Figure 17, the solid red line represents the plastic strain values measured using the method shown in Figure 15, and the dashed blue line represents the predicted average plastic strain values of the spherical cap structure based on Figure 16 and Equation (14).

As shown in Figure 17, the plastic strain values gradually increased from the peripheral circular boundary of the spherical cap shape to the central point. A maximum plastic strain of 0.082 was observed at the central point.

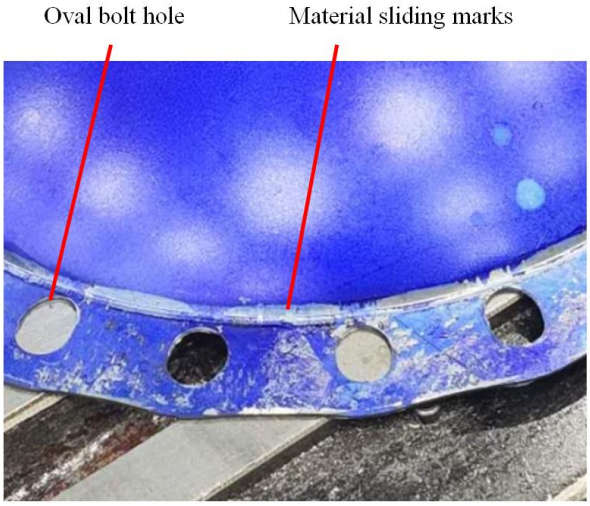

Figure 18. *Internal flow phenomenon of the material in the fixed boundary area.*

Additionally, the average plastic strain value of 0.077 predicted by Equation (14) was slightly larger than the actual measured plastic strain value of 0.070. It was found that the internal flow phenomenon of the material at the peripheral boundary fixed part of the spherical cap structure occurred during free-bulge forming. This trend can be observed in Figure 18, where the circular holes transformed into elliptical shapes after free-bulge forming and there were slip marks at the connection between the spherical cap shape and the flange section.

3.3. Shape Accuracy in the Formed Spherical Cap Structure

To verify the shape accuracy of the spherical cap structure obtained using the free-bulge forming method, an experimental setup was created to measure the external surface shape, as shown in Figure 19.

The measurement device comprised two main parts: an acrylic table that moved primarily in the horizontal direction, as shown in Figure 19 (a), and a laser displacement meter fixed to a stand.

The following step-wise procedure was followed for shape measurement:

1) The spherical cap structure was placed on an acrylic table. While observing the distance readings from the laser displacement meter, the spherical cap structure was moved back and forth and left and right. The product was stopped when the minimum distance was red.
2) As shown in Figure 19 (b), the table was moved horizontally to align with the markings on the ruler and then stopped.
3) As shown in Figure 19 (c), the vertical distance was read from the laser displacement meter to the measurement point on the surface of the spherical cap structure.

The contour shape along the diameter of the spherical cap structure was obtained by repeatedly following steps (2) and (3). The coordinate values of the contour shape of the spherical cap structure in the diameter direction were read from the horizontal moving table and ruler. The coordinate values in the height direction of the contour shape were obtained using a laser displacement meter.

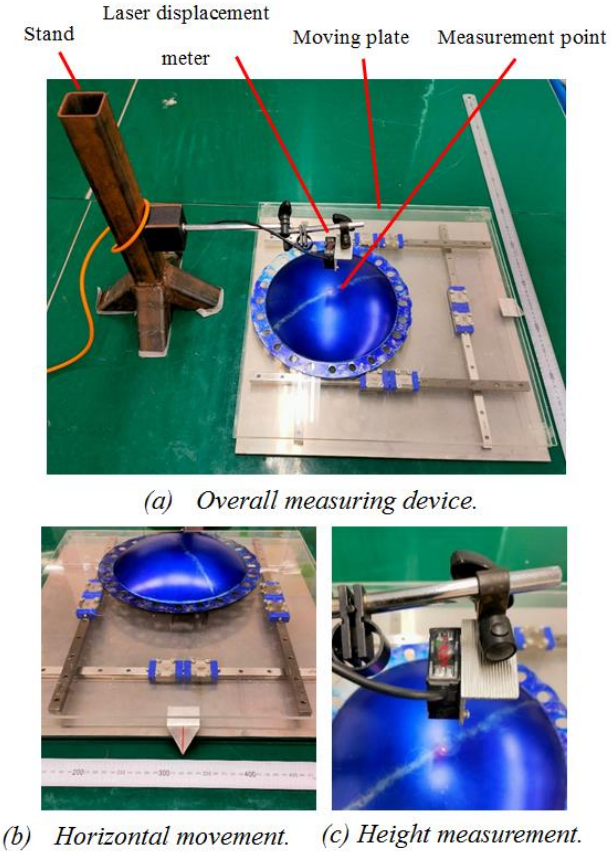

(a) Overall measuring device.

(b) Horizontal movement. (c) Height measurement.

Figure 19. *Measuring device for the external surface shape of spherical cap structure.*

As shown in Figure 19, the external shape of the spherical cap structure was measured and the resulting contour shape data were compared with the theoretically calculated results, as summarized in Figure 20. In Figure 20, the dashed red line represents the actual measured surface shape of the spherical cap structure, whereas the solid black line represents the spherical cap shape obtained through theoretical calculations.

As shown in Figure 20, the measured surface shape of the spherical cap structure obtained using the free-bulge forming method closely matched the theoretically calculated spherical cap shape. For a free-bulge forming height of 45 mm, the maximum height deviation across the surface of the formed spherical cap structure was 1.03 mm, and the maximum relative error was 2.3%. This indicates that the free-bulge forming method provides a high degree of accuracy in achieving the desired spherical cap shape.

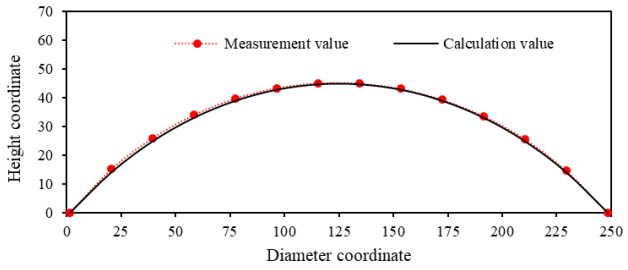

Figure 20. *Measurement results of the surface shape of the spherical cap structure.*

3.4. Thickness Distribution in the Formed Spherical Cap Structure

To investigate the thickness distribution of the spherical cap structure obtained using the free-bulge forming method, the following steps were performed:

1) As shown in Figure 21(a), a perpendicular section of the spherical cap product was cut along the diameter direction using a laser cutting machine.
2) Subsequently, as shown in Figure 21(b), a dial caliper gauge was used to measure the thickness of the cut spherical cap structure along the diameter.

The measured thickness distribution of the spherical cap structure is shown in Figure 22, with red markers indicating the measurement points. It was observed that, compared with the initial thickness of 1 mm before free-bulge forming, the thickness of the formed spherical cap structure generally decreased, with a tendency to follow an axisymmetric distribution around the central axis.

The thickness near the peripheral boundary of the spherical cap structure was relatively larger, with a maximum thickness of 0.981 mm. The thickness at the central point of the spherical cap structure was the lowest, with a minimum thickness of 0.876 mm.

However, the FEM analysis results shown in Figure 12 indicate that the maximum thickness was 0.858 mm and the minimum thickness was 0.965 mm. In comparison, the actual measured values of the free-bulge formed spherical cap

structures were larger.

This discrepancy can be attributed to the internal material flow phenomenon observed in the surrounding boundary fixed part of the spherical cap structure during the actual free-bulge forming process, as shown in Figure 18. This material flow can lead to variations in the thickness distribution that are not fully captured by the FEM model, resulting in thicker regions near the edges and a more uniform distribution in the actual structure. The FEM model assumes idealized behavior, which may not account for the practical material flow occurring during the free-bulge forming process.

For the same reason, the actual average thickness of the free-bulge formed spherical cap structure (0.985 mm) was larger than the calculated average thickness of 0.890 mm obtained using Equation (7). This difference can be attributed to the internal material flow phenomenon observed during the actual free-bulge forming process. This effect is not fully captured by the simplified calculations in Equation (7), which assumes idealized conditions without accounting for the real-world behavior of the material during forming. Therefore, the actual measured average thickness was higher than the predicted value.

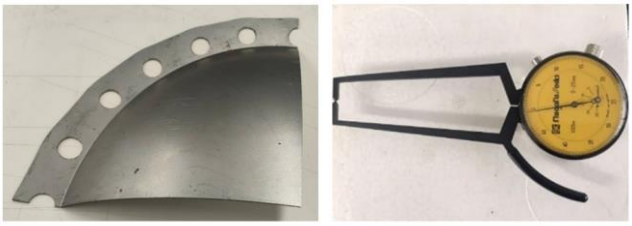

(a) Cut part. (b) Dial caliper gauge.

Figure 21. *Measurement of the thickness distribution of the spherical cap structure.*

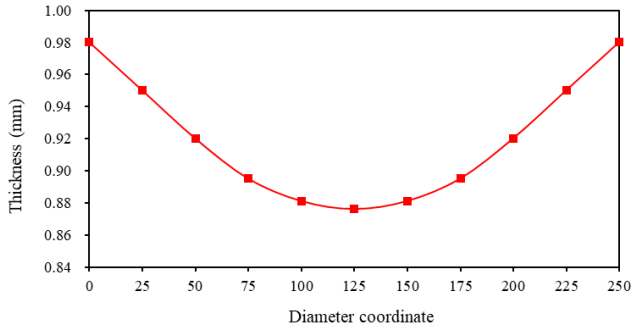

Figure 22. *Measurement results of the thickness distribution of the spherical cap structure.*

4. Conclusion

This study has addressed the processing of thin-walled metallic spherical cap structures and proposed a novel free-bulging forming method. After the theoretical investigations necessary to realize this method, the proposed free-bulging forming method was applied to fabricate spherical cap structures, and detailed examinations were conducted. The following conclusions were drawn:

1) Effectiveness of the Novel Free-bulge Forming Method: The proposed free-bulge forming method was confirmed as a promising technique for efficiently and accurately forming thin-walled metallic spherical cap structures. By appropriately controlling the internal water pressure during the forming process, a uniform spherical cap shape was formed, and plastic deformation proceeded as predicted.
2) Agreement Between Theoretical Investigations and Experimental Results: The theoretical calculations using the proposed equations agreed well with the actual results of the forming experiments. From the FEM analysis and experiments with a manual hydraulic pump, it was confirmed that the shape, plastic strain, and thickness distribution of the spherical cap structure after free-bulge forming were consistent with the predicted values, demonstrating the high precision of the proposed method.
3) Analysis of Plastic Deformation and Thickness Distribution: After free-bulging, the spherical cap structure showed a trend of uniform thickness reduction compared to the pre-formed plate, with the central part being the thinnest. Analysis of the post-forming thickness distribution confirmed that plastic deformation proceeded appropriately, and the material flowed without waste. The reduction in thickness near the edges was minimal, indicating appropriate distribution of the material during the forming process.
4) Shape Accuracy After Forming: The actual shape of the spherical cap structure was also in good agreement with the theoretically calculated results. The surface shape measurement error after forming was within a maximum of 2.3%, which is within the practical range. This indicates that the free-bulge forming method can produce spherical cap structures with high accuracy.
5) Evaluation and Prediction of Plastic Strain: The plastic strain of the spherical cap structure was measured, with a maximum strain of 0.082 occurring at the center after forming. A comparison of the theoretical average strain values with the measured results showed a high prediction accuracy.
6) Potential Practical Applications: The insights gained in this study provide a foundation for mass production and precise processing of thin-walled metallic spherical cap structures. This study paves the way for the practical applications of the free-bulge forming method as a new processing technology in future manufacturing industries.
7) Implications for Future Research: By utilizing the free-bulging method developed in this study, it has been demonstrated that spherical cap products can be plas-

tically formed with high precision without the need for forming dies. This provides a valuable foundational result for future advancements in precision processing and product lightweighting.

Based on the findings of this study, the proposed free-bulge forming method is effective for high-precision processing of thin-walled metallic spherical cap structures, and its industrial application is expected in the future.

Abbreviations

FEM	Finite Element Method
SPCC	Steel Plate Cold Commercial

Author Contributions

Junfu Hou: Validation, Writing – Original Draft

Lingzhe Meng: Data curation, Methodology

Chenghai Kong: Data curation, Investigation, Methodology

Jingchao Guan: Writing – review & editing, Methodology

Wei Zhao: Conceptualization, Writing – editing, Software

Xilu Zhao: Conceptualization, Writing – review

Funding

This work is not supported by any external funding.

Data Availability Statement

Not applicable.

Conflicts of Interest

The authors declare no conflicts of interest.

References

[1] Stoicescu, A. A., Ripeanu, R. G., Tanase, M., & Toader, L. (2025) Current Methods and Technologies for Storage Tank Condition Assessment: A Comprehensive Review. Materials, 18(1074). https://doi.org/10.3390/ma18051074

[2] Cirimello, P. G., Otegui, J. L., Ramajo, D., & Carfi, G., (2019). A major leak in a crude oil tank: Predictable and unexpected root causes. Engineering Failure Analysis, 100, 456-469. https://doi.org/10.1016/j.engfailanal.2019.02.005

[3] Bagarello, S., Campagna, D., & Benedetti, I., (2024). A survey on hydrogen tanks for sustainable aviation. Green Energy and Intelligent Transportation, 100224. https://doi.org/10.1016/j.geits.2024.100224

[4] Milovanovic, A., & Sedmak, A., (2018). Integrity assessment of ammonia spherical storage tank. Procedia Structural Integrity, 13, 994-999. https://doi.org/10.1016/j.prostr.2018.12.185

[5] Lee, H. S., Yoon, J. H., Park, J. S., & Yi, Y. M., (2005). A study on failure characteristic of spherical pressure vessel. Journal of Materials Processing Technology 164, 882-888. https://doi.org/10.1016/j.jmatprotec.2005.02.208

[6] Malfroy, J., Steelant, J., & Vandepitte, D., (2025). A Design Guide to Tapered Conformable Pressure Tanks for Liquid Hydrogen Storage. Aerospace, 12(190). https://doi.org/10.3390/aerospace12030190

[7] Chatterji, S., Butenweg, C., & Klinkel, S., (2025). Unified force-based design approach for the seismic analysis and design of liquid storage tanks. Bulletin of Earthquake Engineering, 2025. https://doi.org/10.1007/s10518-025-02135-8

[8] Drawer, C., Baetcke, L., Lange, J., Shang, Y., & Kaltschmitt, M., (2025). Novel concepts for metal hydride storage tanks - Numerical modeling, simulation and evaluation. Energy Conversion and Management, 327(119572). https://doi.org/10.1016/j.enconman.2025.119572

[9] Arabzadeh, V., Niaki, S. T. A., & Arabzadeh, V., (2018). Construction cost estimation of spherical storage tanks: artificial neural networks and hybrid regression - GA algorithms. Journal of Industrial Engineering International, 14, 747-756. https://doi.org/10.1007/s40092-017-0240-8

[10] Oyelami, A. T., & Olusunle, S. O. O., (2019). Spherical Storage Tank Development Through Mathematical Modeling of Constituent Sections. Mathematical Modelling of Engineering Problems, 6(3), 467-473. https://doi.org/10.18280/mmep.060320

[11] Chen, B, Huang, J. X., & Shen, Y, (2015). The Economic Design and Analysis for Mixed Model Spherical Tank Shell Angle Partition. Procedia Engineering, 130, 41-47. https://doi.org/10.1016/j.proeng.2015.12.173

[12] Demir, K, U, Gokdag, I., Dagkolu, A., & Sahin, M, (2023). Shape and Size Optimization of an Aerospace Propellant Tank. 12th ANKARA International Aerospace Conference 13-15 Sep. 2023 Ankara TURKIYE, AIAC-2023-046.

[13] Yu, Y., Xie, F., Zhu, M., Shuai Yu, S., & Li, Y., (2023). Design and Optimization of the Insulation Performance of a 4000 m3 Liquid Hydrogen Spherical Tank. Processes, 11(1778). https://doi.org/10.3390/pr11061778

[14] Ibrahim, A., Ryu, Y., & Saidpour, M., (2015). Stress Analysis of Thin-Walled Pressure Vessels. Modern Mechanical Engineering, 5, 1-9. https://doi.org/10.4236/mme.2015.51001

[15] Adeyefa, O., & Oluwole, O., (2011). Finite Element Analysis of Von-Mises Stress Distribution in a Spherical Shell of Liquified Natural Gas (LNG) Pressure Vessels. Engineering, 3, 1012-1017. https://doi.org/10.4236/eng.2011.310125

[16] Adibi-Asl, R., & Livieri, P., (2007). Analytical Approach in Autofrettaged Spherical Pressure Vessels Considering the Bauschinger Effect. Journal of Pressure Vessel Technology, 129, 411-419. https://doi.org/10.1115/1.2748839

[17] Luo, Y., Wang, Z., Wang, Q., Mao, H., Hong, Q., & Li, L., (2023). Improvement in Connecting the Structure of Spherical Crown Middle Head. Journal of Physics: Conference Series, 2450(012029). https://doi.org/10.1088/1742-6596/2450/1/012029

[18] Doan, M. L., Nguyen, V. T., & Tran, C. T., (2021). An analysis of In-Vessel Melt Retention strategy for VVER-1000 considering the effect of torospherical lower head vessel. Nuclear Engineering and Design, 371(110972). https://doi.org/10.1016/j.nucengdes.2020.110972

[19] Salman, M. A., Ismail, M. R., & Kahtan, Y. Y., (2018). Effect of Head Types on the Free Vibration and Fatigue for Horizontal LPG Pressure Vessels. Al-Nahrain Journal for Engineering Sciences, 21(04), 494-500. https://doi.org/10.29194/NJES.21040494

[20] Emegbetere, E., ThankGod, B., Oreko, B. U., Akene, A., Oghenekowho, P. A., Edward, B. A., (2021). Design and Analysis of a Butt Welded Pressure Vessel Reactor. Journal of Energy Technology and Environment, 3(2), 71-77. https://doi.org/10.37933/nipes.e/3.2.2021.8

[21] Dandekar, A., Gordon, A., & Kulkarni, M., (2023). Numerical Analysis of Permanent Deformation in Pressure Vessels DUE to Weld Overlay. Proceedings of the ASME 2023 Pressure Vessels & Piping Conference (PVP2023), July 16-21, 2023, Atlanta, Georgia, USA.

[22] Liu, C., & Bhole, S. D., (2002). Fracture behavior in a pressure vessel steel weld. Materials and Design, 23, 371-376. https://doi.org/10.1016/S0261-3069(02)00004-3

[23] Vukojevic, N., Sabanovic, K., Barlov, A., & Rijeci, K., (2023). Application of the Planned Experiment for Determining the Stress Intensity Factor in Vessel Heads Using FEM Analysis. Masinstvo, 3-4(20), 69-76. https://doi.org/10.62456/JMEM.2023.04.069

[24] Vasileiou, A. N., Smith, M. C., Francis, J. A., Balakrishnan, J., Wang, Y. L., Obasi, G., Burke, M. G., Pickering, E. J., Gandy, D. W., & Irvine, N. M., (2021). Development of microstructure and residual stress in electron beam welds in low alloy pressure vessel steels. Materials & Design, 209, 109924. https://doi.org/10.1016/j.matdes.2021.109924

[25] Nie, C., & Dong, P., (2015). A Thermal Stress Mitigation Technique for Local Postweld Heat Treatment of Welds in Pressure Vessels. Journal of Pressure Vessel Technology, 137, 051404. https://doi.org/10.1115/1.4029097

[26] Rathod, D. W., Pandey, S., Singh, P. K., & Prasad, R., (2016). Mechanical Properties Variations and Comparative Analysis of Dissimilar Metal Pipe Welds in Pressure Vessel System of Nuclear Plants. Journal of Pressure Vessel Technology, 138, 011403. https://doi.org/10.1115/1.4031129

[27] Wang, Z. R., Liu, G., Yuan, S. J., Teng, B. G., & He, Z. B., (2005). Progress in shell hydroforming. Journal of Materials Processing Technology, 167(2-3), 230-236. https://doi.org/10.1016/j.jmatprotec.2005.05.045

[28] Bell, C., Corney, J., Zuelli, N., & Savings, D., (2020). A state of the art review of hydroforming technology - Its applications, research areas, history, and future in manufacturing. International Journal of Material Forming, 13, 789-828. https://doi.org/10.1007/s12289-019-01507-1

[29] Yuan, S. J., (2021). Fundamentals and Processes of Fluid Pressure Forming Technology for Complex Thin-Walled Components. Engineering, 7, 358-366. https://doi.org/10.1016/j.eng.2020.08.014

[30] Wang, Z. R., Dai, K., Yuan, S. J., Zeng, Y., & Zhang X., (2000). The development of integral hydro-bulge forming (IHBF) process and its numerical simulation. Journal of Materials Processing Technology, 102(1-3), 168-173. https://doi.org/10.1016/S0924-0136(00)00406-4

[31] Zhang, S. H., Zeng, Y. S., & Wang, Z. R., (1996). Theoretical analysis and experimental research into the integral hydro-bulge forming of oblate shells. Journal of Materials Processing Technology, 62(1-3), 199-205. https://doi.org/10.1016/0924-0136(95)02230-9

[32] Wu, W., & Wang, Z. R., (2004). Deformation analyses of the integrated hydro-bulge forming of a spheroidal vessel from different preform types. Journal of Materials Processing Technology, 151(1-3), 275-283. https://doi.org/10.1016/j.jmatprotec.2004.04.112

[33] Polyanin, A. D., & Manzhirov, A. V., (2007). Handbook of Mathematics for Engineers and Scientists. Chapman & Hall/CRC Taylor & Francis Group, 69-70.